Computation of the lattice Green function for a dislocation

Anne Marie Z. Tan and Dallas R. Trinkle

Phys. Rev. E **94**, 023308 — Published 11 August 2016

DOI: 10.1103/PhysRevE.94.023308

Computation of the lattice Green function for a dislocation

Anne Marie Z. Tan and Dallas R. Trinkle*

Department of Materials Science and Engineering,

University of Illinois at Urbana-Champaign, Urbana, IL 61801, USA

(Dated: July 1, 2016)

Abstract

Modeling isolated dislocations is challenging due to their long-ranged strain fields. Flexible boundary condition methods capture the correct long-range strain field of a defect by coupling the defect core to an infinite harmonic bulk through the lattice Green function (LGF). To improve the accuracy and efficiency of flexible boundary condition methods, we develop a numerical method to compute the LGF specifically for a dislocation geometry; in contrast to previous methods, where the LGF was computed for the perfect bulk as an approximation for the dislocation. Our approach directly accounts for the topology of a dislocation, and the errors in the LGF computation converge rapidly for edge dislocations in a simple cubic model system as well as in BCC Fe with an empirical potential. When used within the flexible boundary condition approach, the dislocation LGF relaxes dislocation core geometries in fewer iterations than when the perfect bulk LGF is used as an approximation for the dislocation, making a flexible boundary condition approach more efficient.

* dtrinkle@illinois.edu

I. INTRODUCTION

Defects such as point defects, dislocations, interfaces, and grain boundaries play key roles in determining material properties [1] and knowledge of their geometries is important to model them accurately. The far-field geometry of many defects can be well described by anisotropic continuum elasticity theory [2, 3], but atomistic methods such as density functional theory (DFT) are needed to accurately determine the geometry within the defect core, where the elastic solution diverges. Modeling defects such as isolated dislocations is challenging because their long-range strain fields are incompatible with periodic or fixed boundary conditions. Some DFT-based methods that have been used to model dislocation core structures are reviewed in [4]. One way to circumvent the issues associated with modeling isolated dislocations is to compute periodic arrays of dislocation dipoles [5, 6] or quadrupoles [7, 8]. Alternatively, isolated dislocations can be directly simulated using multiscale methods that capture the long-range strain field of the defect by coupling the quantum mechanical core to a continuum.

Many different coupling approaches have been developed, for example, using finite elements [9, 10], classical potentials [11, 12], or flexible boundary conditions (FBC) which displace atoms outside the defect core according to the lattice Green function (LGF)[13]. These approaches are all based on the same concept of using a different Hamiltonian for atoms in the dislocation core than for those outside the core. A more accurate but computationally demanding method like DFT is used in the highly distorted dislocation core region, while a faster but less accurate method which captures the far-field response of the dislocation is used outside the core. However, there are a few key differences between the various coupling approaches. The FBC and finite element approaches ensure that the surrounding region has the same elastic properties as the core by deriving the force-constants required to compute the LGF and the finite element constitutive equations from DFT [9, 14]. Coupling DFT to a classical potential is trickier—available potentials may not have been fit to reproduce the relevant DFT quantities (force constant matrix, lattice and elastic constants, and higher derivatives), leading to an unphysical mismatch in material behavior across the coupling interface which can introduce substantial errors in the simulation [12]. Another difference is that in the classical potential and finite element approaches, the region described by the classical potential or finite elements is finite and appropriate boundary conditions must be

applied at the outer boundary of the simulation. In contrast, the LGF used in the FBC method smoothly transitions into the continuum elastic Green function at large distances [15, 16], effectively embedding the defect within an infinite bulk. In this work, we focus on the FBC method, which has been applied with DFT to relax isolated screw and edge dislocations [17–20].

The accuracy and efficiency of the FBC method depends on the accuracy of the LGF. Analytic results for LGF of simple systems such as cubic lattices with nearest-neighbor interactions are known [21, 22]. Recently, computation of the LGF for a perfect bulk crystal by inversion of the force-constant matrix was demonstrated for Bravais lattices [23], and later extended to crystals with multiple-atom basis [24] or even a planar interface[25]. However, difficulties may arise when applying the LGF for the bulk as an approximation to a lattice containing a line defect. The LGF for the perfect bulk crystal gives the response between atoms connected in the perfect lattice topology; however, the topology of atoms in a distorted lattice can deviate significantly from that of the perfect lattice. In such cases, the bulk LGF may not capture the response between atoms in the distorted lattice accurately, which could lead to slower convergence.

We develop a method to compute the LGF specifically for a dislocation geometry. Section II reviews the harmonic lattice response functions—the force-constant matrix and LGF—and the FBC method. We develop a numerical method to compute the LGF for a dislocation geometry in Section III. In Sections IV and V, we apply our new method for computing the LGF to edge dislocations in a simple cubic model system and BCC Fe, respectively. We show that the dislocation LGF captures the response of atoms in the dislocation geometry more accurately than the perfect bulk LGF, and when used within the FBC approach, relaxes dislocation core geometries in fewer iterations than when the bulk LGF is used.

II. HARMONIC LATTICE RESPONSE

Atoms in a crystal displace in response to external or internal forces; conversely, displacing atoms from their equilibrium positions generates forces. For small forces and displacements, the atoms behave harmonically and the two quantities are linearly related. The infinite harmonic crystal has been well studied in both classical and quantum theory [26, 27]. For a crystal containing N atoms, the $3N \times 3N$ force-constant matrix $D_{\alpha\beta}(\vec{R}_i, \vec{R}_j)$ relates the

α-component of the force on atom i located at position $\vec{R}_i$, $f_\alpha(\vec{R}_i)$, to the β-components of the displacements on atoms j at positions $\vec{R}_j$, $u_\beta(\vec{R}_j)$, as

$$f_\alpha(\vec{R}_i) = -\sum_{j,\beta} D_{\alpha\beta}(\vec{R}_i, \vec{R}_j) u_\beta(\vec{R}_j), \tag{1}$$

where α and β are Cartesian directions, and $D_{\alpha\beta}(\vec{R}_i, \vec{R}_j)$ is given by the second derivative of the total potential energy U^{total},

$$D_{\alpha\beta}(\vec{R}_i, \vec{R}_j) = \frac{\partial^2 U^{\text{total}}}{\partial u_\alpha(\vec{R}_i)\, \partial u_\beta(\vec{R}_j)}. \tag{2}$$

A perfect crystal has translational symmetry, so the force-constant matrix depends only on the difference of positions $\vec{R_{ij}}$ between atoms i and j: $D_{\alpha\beta}(\vec{R}_i, \vec{R}_j) = D_{\alpha\beta}(\vec{R}_i - \vec{R}_j) = D_{\alpha\beta}(\vec{R_{ij}})$. In addition, $D_{\alpha\beta}(\vec{R_{ij}}) = D_{\beta\alpha}(\vec{R_{ji}}) = D_{\beta\alpha}(\vec{R_{ij}})$ due to independence of differentiation order and inversion symmetry of Bravais lattices. The lattice Green function $G_{\alpha\beta}(\vec{R}_i, \vec{R}_j)$ relates the displacement $u_\alpha(\vec{R}_i)$ on atom i located at position $\vec{R}_i$ to the forces $f_\beta(\vec{R}_j)$ on atoms j at positions $\vec{R}_j$ as

$$u_\alpha(\vec{R}_i) = -\sum_{j,\beta} G_{\alpha\beta}(\vec{R}_i, \vec{R}_j) f_\beta(\vec{R}_j), \tag{3}$$

The LGF obeys the same symmetries as the force-constant matrix: $G_{\alpha\beta}(\vec{R}_i, \vec{R}_j) = G_{\alpha\beta}(\vec{R_{ij}}) = G_{\beta\alpha}(\vec{R_{ji}}) = G_{\beta\alpha}(\vec{R_{ij}})$, with the last equality only being valid for Bravais lattices. As $|R_{ij}| \to \infty$, the LGF approaches the elastic Green function (EGF) from continuum elasticity [21–24]. The LGF and force-constant matrix are inverses of each other,

$$\sum_{k,\gamma} G_{\alpha\gamma}(\vec{R}_i, \vec{R}_k) D_{\gamma\beta}(\vec{R}_k, \vec{R}_j) = \delta_{ij}\delta_{\alpha\beta}, \tag{4}$$

where δ is the Kronecker delta. By Newton's third law, no forces are generated under a uniform translation of the entire system, so the force-constant matrix obeys the sum rule $\sum_{\vec{R}_j} D(\vec{R}_i, \vec{R}_j) = 0$, and is a singular matrix. Hence, the LGF and force-constant matrix are pseudoinverses of each other.

The FBC method couples atomistic relaxation within the dislocation core with LGF relaxation outside the core in order to efficiently relax isolated defect geometries. Figure 1 shows the division of the area around a dislocation into the different regions required for applying FBC (regions 1, 2 and 3 only) as well as for computing the LGF (all regions shown). Region 1 contains atoms very close to the dislocation core whose interactions are

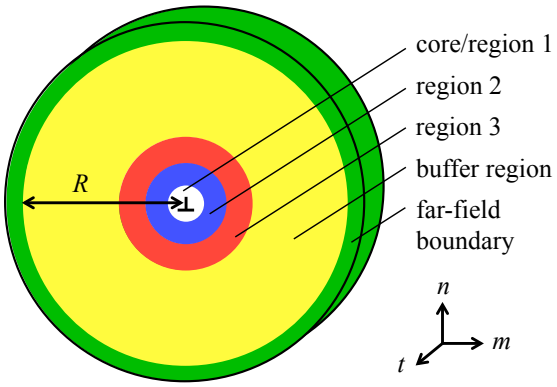

FIG. 1. (Color online) Schematic showing the system setup used in the flexible boundary condition (FBC) approach (regions 1–3 only), as well as to calculate the lattice Green function (LGF) (all regions shown). Region 1 (white) contains the highly distorted dislocation core (indicated by the $\perp$) which will be relaxed by atomistic methods. Region 2 (blue) contains atoms which will have forces due to the displacements in region 1. Regions 1, 2 and 3 (red) contain the atoms which will be displaced according to the LGF in the FBC approach. The buffer region (yellow) and the far-field boundary region (green) are not required for the implementation of FBC, but are used in our computation of the LGF. Atoms within the far-field boundary region are far away from the core and are displaced according to the elastic Green function (EGF). The buffer region of radius R allows for the LGF to approach the EGF in the far-field. The regions are defined in the dislocation coordinate system, where $\vec{t}$ is the dislocation threading direction, and $\vec{m}$ and $\vec{n}$ are perpendicular vectors in the plane normal to $\vec{t}$.

nonlinear due to large lattice distortions, which we relax atomistically. Region 2 includes all atoms on which a force may be exerted by any atom in region 1. Region 3 contains atoms which might experience a force from atoms in region 2. Therefore, the thickness of regions 2 and 3 should each be at least equal to the range of the interactions between atoms in the system. The FBC approach consists of two steps: in the first step, we relax atoms in the defect core (region 1) using conjugate gradient with an atomistic method such as classical potentials or density functional theory, while holding the atoms in regions 2 and 3 fixed. Since later steps will disturb the atoms in region 1, we do not fully relax region 1. Instead, only a small number of conjugate gradient step are performed during each core relaxation, which makes early iterations of this step more efficient while still ensuring accuracy in the final iteration since the final relaxation should only require small adjustments. Displacing

atoms in region 1 generates forces on atoms in region 2, which we relax in the LGF update step by displacing atoms in regions 1, 2 and 3 according to the LGF. This in turn builds up forces in region 1, so we alternate between these two steps until all forces in regions 1 and 2 are smaller than a defined tolerance.

In addition to the three regions discussed above, our method for computing the LGF requires defining two additional regions around the dislocation—the buffer region and the far-field boundary. The far-field boundary contains atoms far away from the core whose displacements we approximate using the bulk EGF. Strictly speaking, this assumption is only valid for perfect bulk crystals; when defects are present, the long-range behavior of the defect LGF is not necessarily given by the bulk EGF [28, 29]. However, for the systems that we have considered, we find that the errors due to this approximation are sufficiently small to consider this approximation reasonable (c.f., Figs. 5 and 9). Like regions 2 and 3, the thickness of the far-field boundary is determined by the range of the interactions between atoms, so that all atoms whose displacements could generate forces in the buffer region are fully contained within our system setup. The buffer region contains the remaining atoms between region 3 and the far-field boundary and its size R can be varied; increasing R pushes the far-field boundary further away from the dislocation core, making the approximation of the far-field displacements more accurate.

III. METHODS FOR COMPUTING THE LATTICE GREEN FUNCTION

A. Computing the LGF for the dislocation geometry including region 1

The FBC approach described in the previous section, requires the computation of the LGF for displacements in regions 1, 2 and 3 due to forces in region 2. We start by partitioning the force-constant matrix and LGF as follows:

$$D = \left(\begin{array}{c|c} D^{\mathrm{ii}} & D^{\mathrm{io}} \\ \hline D^{\mathrm{oi}} & D^{\mathrm{oo}} \end{array}\right), \qquad G = \left(\begin{array}{c|c} G^{\mathrm{ii}} & G^{\mathrm{io}} \\ \hline G^{\mathrm{oi}} & G^{\mathrm{oo}} \end{array}\right), \tag{5}$$

where the superscripts i and o refer to atoms on the "inside", i.e. regions 1, 2, 3 and buffer, and atoms on the "outside", i.e. far-field boundary region, respectively. For example, D^{io} is the block of the force-constant matrix that gives forces on "inside" atoms due to displacements on "outside" atoms. Since D and G are the pseudoinverse of each other, we

have

$$D^{\text{ii}}G^{\text{ii}} + D^{\text{io}}G^{\text{oi}} = \mathbf{1}. \tag{6}$$

We approximate D^{ii} and D^{io} for the dislocation geometry using a few different approaches which we discuss in the next paragraph. We use the EGF (G^E) to approximate G^{oi} between atoms in the far-field and region 2. We then solve for G^{ii} according to

$$G^{\text{ii}} = (D^{\text{ii}})^{-1}(\mathbf{1} - D^{\text{io}}G^E). \tag{7}$$

We compute each column of G^{ii} numerically by first applying a unit force f on an atom in region 2 and determining the far-field displacements $u^{\text{far-field}} = -G^E f$ due to that force. We then evaluate the forces on atoms in the buffer region $f^{\text{buffer}} = -D^{\text{io}}u^{\text{far-field}} = D^{\text{io}}G^E f$ generated by the far-field displacements, and use conjugate gradient to solve for the displacement field corresponding to the effective forces in the system, $f^{\text{eff}} = (\mathbf{1} - D^{\text{io}}G^E)f$. This gives us the LGF due to the initial applied force. By systematically looping through every atom in region 2 in this way, we can compute the portion of the G^{ii} matrix that gives displacements in regions 1, 2 and 3 due to forces in region 2. As we treat all interactions harmonically, this approach is computationally efficient and the only approximations are the harmonic interaction, and the use of the elastic Green function for the far-field.

We consider three different approaches to estimate D for the dislocation geometry. Unlike the LGF, the force-constants are short-range, and so each atom only interacts with its local environment, which can be bulk-like even close to a dislocation. Therefore, we can make a simple approximation for the force-constants between a pair of atoms i and j in the dislocation geometry by using the force-constants from the closest equivalent pair of atoms i' and j' in the bulk,

$$D^{\text{disl,bulk-like}}(\vec{R}_i, \vec{R}_j) = D^{\text{bulk}}(\vec{R}_{i'}, \vec{R}_{j'}). \tag{8}$$

We can improve on this approximation by considering the effects of local strains in the dislocation geometry:

$$\begin{aligned} D^{\text{disl,str}}(\vec{R}_i, \vec{R}_j) = {} & D^{\text{disl,bulk-like}}(\vec{R}_i, \vec{R}_j) \\ & + \sum_{\alpha,\beta} \bar{\epsilon}_{\alpha\beta}(\vec{R}_i, \vec{R}_j) \cdot \frac{\partial D(\vec{R}_i, \vec{R}_j)}{\partial \epsilon_{\alpha\beta}}, \end{aligned} \tag{9}$$

where α and β are Cartesian directions, $\bar{\epsilon}(\vec{R}_i, \vec{R}_j)$ is the average of the local strains at atoms i and j, and $\partial D/\partial \epsilon_{\alpha\beta}$ is the appropriate strain-derivative of the force-constants. We can

also account for local rotations in the dislocation geometry by rotating D between the pair of atoms,

$$D^{\text{disl,str+rot}}(\vec{R}_i, \vec{R}_j) = \\ \bar{\theta}(\vec{R}_i, \vec{R}_j) \cdot D^{\text{disl,str}}(\vec{R}_i, \vec{R}_j) \cdot \bar{\theta}^{\text{T}}(\vec{R}_i, \vec{R}_j), \tag{10}$$

where $\bar{\theta}(\vec{R}_i, \vec{R}_j)$ is the average of the local rotation around atoms i and j.

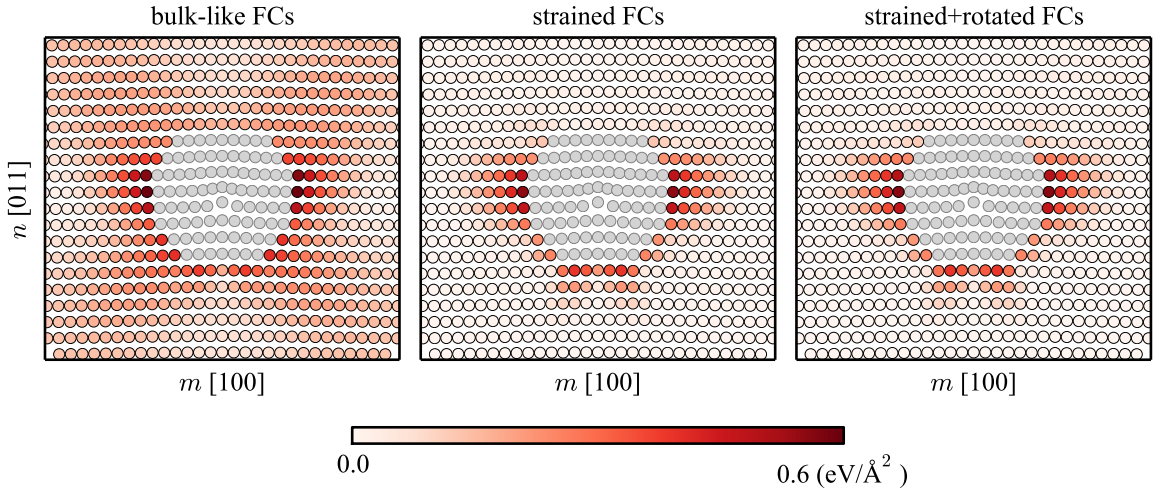

FIG. 2. Errors in the onsite force-constants around a $\langle 100 \rangle \{011\}$ edge dislocation in BCC iron, with respect to the directly computed dislocation force-constants, computed using the different approximations. The shading on each atom indicates the root-mean-square error in that atom's onsite force-constants. We evaluate these errors for atoms in region 2 and region 3 but not for region 1, since we do not expect the harmonic approximation to be valid that close to the dislocation core. Instead, the region 1 atoms are filled in with grey. The error in the bulk-like force-constants (left) has a long range component that decays as $1/R$. This component of the error is eliminated when we account for the local strains and rotations. The strained (center) and strained and rotated (right) approximations give very similar force-constants.

Figure 2 compares the accuracy of the different approximations for force-constants around a $\langle 100 \rangle \{011\}$ edge dislocation in BCC iron. In order to quantify the errors in each of the approximations described above, we compute the full dislocation force-constants by displacing each atom in the dislocation geometry one at a time and evaluating the resulting forces atomistically. The force-constant matrix obtained from this direct calculation accounts for all geometry effects and therefore gives the most accurate harmonic lattice response of atoms

around the dislocation. However, computing the full dislocation force-constants is computationally expensive, and we only evaluate them here in order to benchmark the accuracy of the various approximate force-constant matrices. The leftmost plot in Fig. 2 shows that the error in the bulk-like force-constants has a long range component that decays like $1/R$. The center and rightmost plots in the figure show that this component of the error is eliminated when local strains and rotations—which also have $1/R$ behavior around a dislocation—are included. The errors in the strained, and strained and rotated approximations are similar, indicating that the effect of local rotations on the force-constants is small. Even after accounting for strain and rotation effects, there are still relatively large errors on atoms close to the core, due to higher-order terms such as anharmonicity that are not included in our simple approximations.

B. Computing the LGF for the dislocation geometry after disconnecting region 1

We also compute the LGF for the case where region 1 is disconnected from the rest of the system, which we use within a modified FBC approach. Similar to the FBC approach described previously, this involves alternating between two steps: first, we relax atoms in the defect core (region 1) using an atomistic method, which generates forces on atoms in region 2. In the LGF update step, we relax these forces by displacing only atoms in regions 2 and 3 according to the LGF, in contrast to the previous case in which we displace all atoms in region 1, 2 and 3. As before, we alternate between these two steps until all forces in regions 1 and 2 are reduced below a chosen tolerance. This approach requires the LGF for displacements in regions 2 and 3 due to forces in region 2, while constraining atoms in region 1 to have no displacements in response to forces in region 2. Therefore, the system of interest becomes one in which region 1 is disconnected from region 2 but not entirely removed. The force-constants between atoms in region 1 and atoms in region 2 in the disconnected system are zero, while the onsite terms are the same as before, resulting in the sum rule being broken, i.e. $\sum_{\vec{R}_j} D(\vec{R}_i, \vec{R}_j) \neq 0$.

We compute the LGF for the disconnected geometry in a similar manner as was previously used to compute the correction to the LGF due to the introduction of point defects [21, 30]. The LGF for the disconnected system is related to the LGF of the system including region

1 according to

$$G = G^0 + \delta G = (D^0 + \delta D)^{-1} = D^{-1}, \tag{11}$$

where G^0 and D^0 are the LGF and force-constant matrix for the full system (computed using the method discussed in the previous section), and δG and δD are the corrections to the LGF and force-constant matrix due to disconnecting region 1. The quantity to be computed is δG, while δD is known and is related to the breaking of bonds between atoms in region 1 and region 2. Rewriting Eq. (11) in the form of a Dyson equation,

$$G = G^0(\mathbf{1} - \delta D G), \tag{12}$$

and making use of the fact that δD is non-zero only for a small and localized group of atoms near the boundary between regions 1 and 2, we compute δG as

$$\delta G = -(\mathbf{1} + G^0 \delta D)^{-1} G^0 \delta D G^0. \tag{13}$$

IV. APPLICATION: SIMPLE CUBIC (SC) MODEL SYSTEM

In this section, we test our methods for computing the LGF by applying them to a simple cubic (SC) model system containing an edge dislocation. We verify that the LGF computed using our method specifically for the edge dislocation geometry captures the response of atoms around the dislocation accurately. We show that using this dislocation LGF leads to faster relaxation when used within the FBC approach, compared to using the bulk LGF. We also study how the errors in the LGF computation converge with system size.

We set up a SC system with unit lattice spacing and atoms connected by first- and second-nearest-neighbor radial springs, both with spring constant of 1. The system is elastically isotropic, with elastic constants $C_{11} = 3, C_{12} = 1$ and $2C_{44} = C_{11} - C_{12} = 1$, or Poisson ratio of 0.25 and shear modulus of 1. For this simple model system, we model the interactions in region 1 using a version of the harmonic potential which modifies the spring constants based on the orientation and length of the springs. To account for the spring orientation, we rotate the force-constant matrix between each pair of first- and second-nearest-neighbor atoms based on their orientation in the dislocation geometry relative to what they would be in the ideal bulk. We introduce a scaling factor to modify the strength of the spring constants based on the distance between each pair of atoms. We construct the scaling factor such that

the strength of the first-nearest-neighbor springs decay gradually for distances greater than the equilibrium first-nearest-neighbor distance, 1.0, becoming zero for distances greater than $\sqrt{2}$, the equilibrium second-nearest-neighbor distance. Similarly, we scale the strength of the second-nearest-neighbor springs so that they decay gradually for distances either less than or greater than $\sqrt{2}$, becoming zero for distances less than 1.0 or greater than 2.0. We generate the initial edge dislocation geometry using the elastic displacement field for an edge dislocation in an isotropic medium [3]. The system setup contains 14 atoms in region 1, 66 atoms in region 2, and 121 atoms in region 3. For this system, we approximate the edge dislocation force-constant matrix using the bulk-like approximation described in Eq. (8).

Figure 3 shows that the errors in displacements due to applying the bulk LGF to a SC system containing an edge dislocation are greatly reduced by using the LGF computed specifically for the appropriate dislocation geometry. To test the accuracy of the displacements generated by each LGF, we construct a test case for which we know the correct displacements. We apply a unit displacement on an atom in region 2, evaluate the forces due to this displacement, then use the LGF computed for the bulk (bulk LGF) and the LGF computed for the edge dislocation (edge LGF) to generate displacements from these forces. As the forces are generated from a displacement, we expect them to generate the same displacement in response. Therefore, the deviation between the initial displacement and the displacements computed by each LGF is a measure of the accuracy of each LGF when applied to the edge dislocation geometry. As discussed briefly in the introduction, we expect the bulk LGF to be a particularly poor approximation between atoms on opposite sides of an edge dislocation where the topology deviates the most from bulk. We observe this in the top figure of Fig. 3, where the largest errors are located on the opposite side (right side) of the dislocation from the forces due to the initial displacement (left side). Using the LGF computed specifically for the edge dislocation geometry eliminates this issue, leading to a more even distribution of errors and reducing the largest errors by more than 3 orders of magnitude compared to when the bulk LGF is used. The remaining errors are due to using the EGF to approximate the far-field displacements when computing the edge LGF, and they scale with system size R as $1/R^2$. The magnitude and convergence behavior of these errors are in agreement with what we observe in Fig. 5. The far-field errors in the computed edge LGF are an order of magnitude larger than that for the bulk LGF because the presence of the edge dislocation causes heterogeneity in the elastic constants that is not

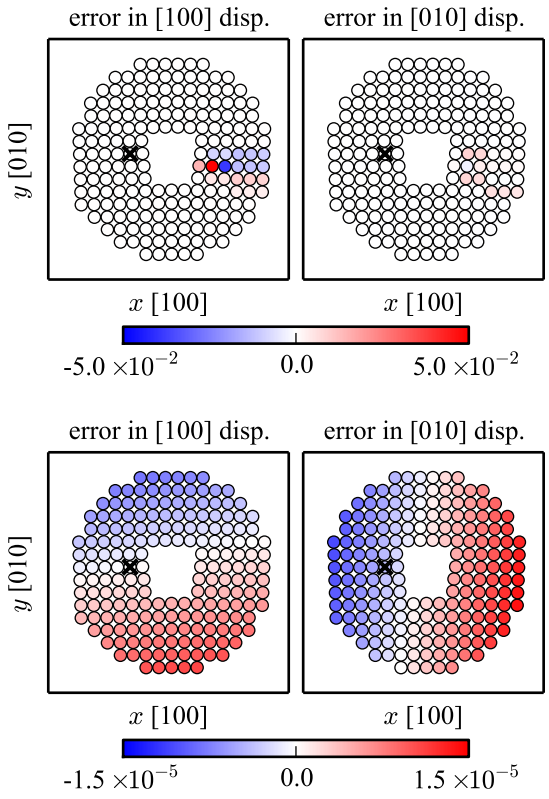

FIG. 3. Error in the displacements generated by the bulk LGF (top) and the edge LGF (bottom) for atoms in a SC edge dislocation geometry. We compute the displacements due to the set of forces that are generated by applying a small displacement in the [100] direction on the atom indicated by the cross. Both the bulk LGF and the edge LGF used to compute the displacements were calculated using system size $R = 60$. The figures show the error in the [100] and [010] directions; this SC edge dislocation has threading vector $\vec{t} = [001]$, so the system is effectively 2-dimensional. In the top figure (using the bulk LGF), 19 atoms which are localized at the opposite side of the edge dislocation from the forces have large errors $> 5.0 \times 10^{-3}$, while the rest of the atoms have errors $< 10^{-5}$. The errors in the bottom figure (using the edge LGF) are all $< 1.5 \times 10^{-5}$. While the figure plots the errors for a specific test case, we have applied test displacements on other atoms as well and the errors are of similar magnitude to those shown here.

accounted for by the EGF used to evaluate the far-field response in both cases.

Figure 4 compares the FBC relaxation of the SC edge dislocation using different LGF, and shows that the edge LGF leads to the fastest convergence to the relaxed geometry. When we displace atoms in regions 1, 2 and 3 during the LGF update step, the edge LGF

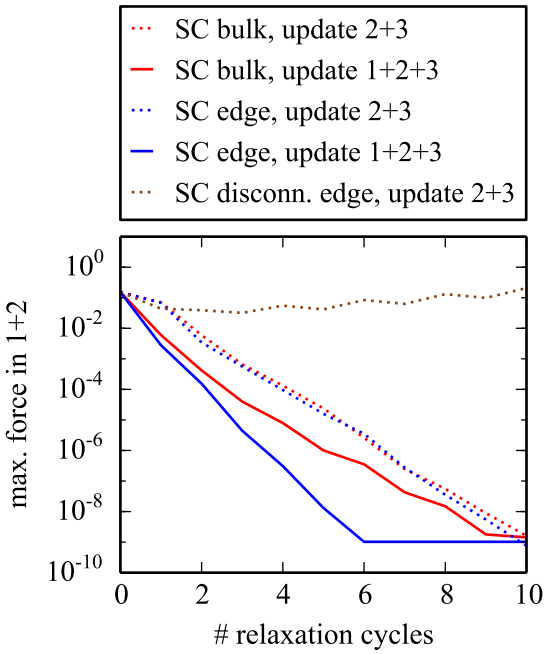

FIG. 4. Comparison of the relaxation of the SC edge dislocation geometry using different LGF. All the LGF used during the relaxations were calculated using system size $R = 60$. Relaxing the edge dislocation with the bulk LGF (red) and the edge LGF (blue), the forces in region 1 and 2 decrease and the geometries converge to the relaxed geometry, with the edge LGF converging faster. Including region 1 in the LGF update step (solid lines) leads to faster convergence than when region 1 is fixed (dotted lines). When relaxing with the disconnected edge LGF (brown), the forces in regions 1 and 2 increase and the geometry does not converge due to the incompatibility in applying the far-field bulk elastic response to the disconnected system.

results in faster convergence to the relaxed geometry as it is able to capture the response of atoms in the dislocation geometry more accurately than the bulk LGF. When we displace only regions 2 and 3 during the LGF update step, the geometries converge slower than when we displace all 3 regions. By fixing the atoms in region 1 and not displacing them during this step, the reduction of forces in region 2 is less effective, leading to the slower overall force convergence. While the relaxations carried out using the bulk and edge LGF converge, the relaxation using the LGF for the edge dislocation geometry with region 1 disconnected ("disconnected edge LGF") does not. We believe that the disconnected edge LGF does not work well because the far-field response of bulk is not compatible with the disconnected system which breaks the sum rule. Our approach for determining the correction to the LGF

only accounts for the local changes in the force-constants without considering the changes in the far-field response due to disconnecting region 1, resulting in the disconnected edge LGF not being computed accurately.

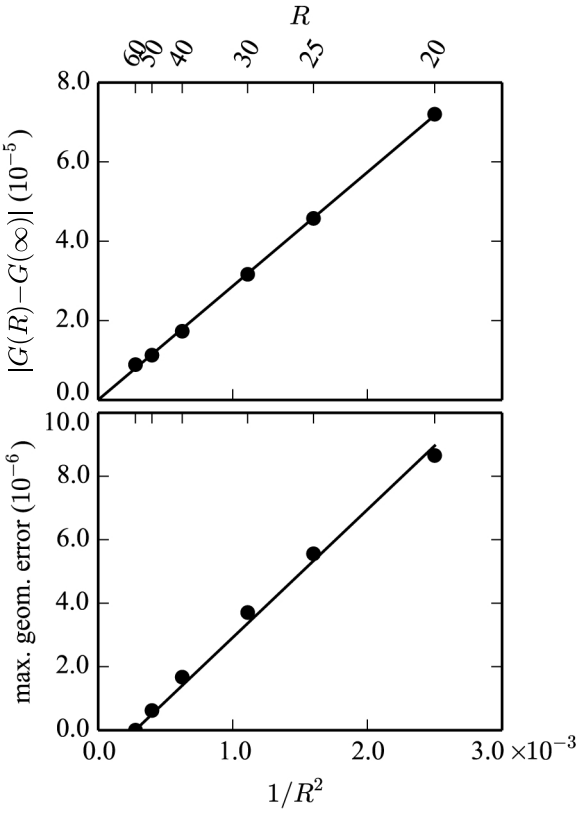

FIG. 5. Convergence behavior of the errors in the computed G (top) and the relaxed edge dislocation geometry (bottom) for the SC model system, with respect to system size R. In each figure, the solid line is the best-fit line through the data points (filled circles). (Top) The vertical axis is the deviation of $G(R = 20, 25, 30, 40, 50, 60)$ from $G(R \to \infty)$. The figure plots the convergence of one specific entry of G; we found that other entries of G show similar convergence behavior as well. (Bottom) The vertical axis is the maximum difference between the geometries obtained from relaxation using $G(R = 20, 25, 30, 40, 50)$ compared to that obtained from using $G(R = 60)$. Both the errors in the computed G and the relaxed edge dislocation geometry are small and converge as $1/R^2$.

Figure 5 shows that the errors in both the computed LGF and the relaxed SC edge dislocation geometries converge as $1/R^2$, where R is the radius of the system up to the buffer region. Our method for computing the LGF involves approximating the displacements of

atoms at the far-field using the EGF, an approximation that gets better for large R. We compute the LGF using different system sizes R—while keeping the size of regions 1, 2 and 3 fixed—and extrapolate the data to estimate the LGF as $R \to \infty$. The errors in the LGF due to the far-field approximation are small (on the order of 10^{-5}), controllable, and converge rapidly as $1/R^2$, which suggests that the approximation we used in the far-field is appropriate for this system. We also investigate the effect of these errors on the accuracy of the relaxed geometries by comparing the geometries relaxed with FBC using LGFs computed with $R = 20, 25, 30, 40, 50$ to that obtained from FBC relaxation using the LGF computed with $R = 60$. We quantify the difference in the geometry around each atom by computing the root-mean-square difference between the vectors from each atom to its neighbors in the different geometries, and plot the maximum value of these local geometry differences as measure of the overall difference in geometry. The differences in the relaxed geometries are also small (on the order of 10^{-6}) and converge rapidly as $1/R^2$.

V. APPLICATION: BCC IRON

In this section, we apply our new method for computing the LGF to the $\langle 100 \rangle \{011\}$ edge dislocation geometry in BCC Fe. As in the SC case, we show that the LGF computed using our method specifically for this edge dislocation geometry captures the response of atoms around the dislocation more accurately than the bulk LGF, leading to faster relaxation when used within the FBC approach. We also study how using different approaches to estimate the force-constants around the dislocation affects the computed LGF and relaxation behavior. Finally, we verify that the errors in the LGF computation converge rapidly with system size.

For computational efficiency during testing, we treat the atoms in the dislocation core region using a classical potential. We use the LAMMPS package [31] with the Mendelev embedded atom method potential for Fe [32] to evaluate the forces and perform the relaxations, and the program PHON [33] to compute the force-constants. For this potential, the lattice constant is $a_0 = 2.8553$ Å and the elastic constants are $C_{11} = 243.4$ GPa, $C_{12} = 145.0$ GPa and $C_{44} = 116.0$ GPa. The system setup contains 84 atoms in region 1, 312 atoms in region 2, and 466 atoms in region 3.

In order to obtain an accurate relaxed geometry using the FBC approach, we must ensure that forces in region 3 of the initial geometry are small. We generate the initial edge dislo-

cation geometry using the elastic displacement field for an edge dislocation in an anisotropic medium [3]. If we generate the initial geometry by simply evaluating the displacements based on the undislocated atom coordinates (i.e. at perfect lattice positions), this results in localized forces on the order of 0.1 eV/Å in region 3 that decay slowly as we move away from the dislocation core. This is undesirable because the FBC approach only relaxes forces in regions 1 and 2, so large forces in region 3 at the end of the relaxation would lead to an inaccurate final geometry. To generate a better initial geometry, we evaluate the displacements based on the final displaced atom coordinates. We do this by iterating the calculation of the displacements until the displacements of each atom from their perfect lattice positions are self-consistent with those given by the anisotropic elastic solution evaluated at the final displaced positions. Sinclair *et al.* discussed the importance of using this approach to set up the initial geometry in their original paper on FBC [13].

Figure 6 shows that the LGF computed specifically for the edge dislocation geometry gives more accurate displacements in response to forces around the dislocation than the bulk LGF. Unless otherwise specified, we refer to the edge LGF computed using the bulk-like approximation for the force-constants (Eq. (8)). We carry out the same tests as in the SC case to determine the error in the displacements generated by each LGF when it is applied to the edge dislocation geometry. However, unlike Fig. 3, Fig. 6 summarizes the results from applying the test displacement on every atom in region 2 that does not generate forces in region 3 or beyond. For each of these atoms outlined in black, the intensity of the shading indicates the maximum error in the displacements computed in response to a set of forces that were generated by applying an initial test displacement on that atom. For the purpose of this test, we evaluate all the forces and displacements—even those in region 1—using the force-constant matrix and LGF, respectively. Therefore, the responses in this harmonic approximate BCC iron system are linear and the errors in the displacements are proportional to the initial displacement. As in the SC case, we find that using the edge LGF instead of the bulk LGF around the edge dislocation geometry reduces the maximum errors by three orders of magnitude, which shows that the edge LGF is better able to capture the response of atoms in the dislocation geometry. Again, the small errors that remain are due to the far-field approximation, and scale with the system size R as $1/R^2$.

We use the bulk and edge LGF within the FBC approach to relax a $\langle 100 \rangle \{011\}$ edge dislocation geometry in BCC Fe, and compare these relaxed geometries against that obtained

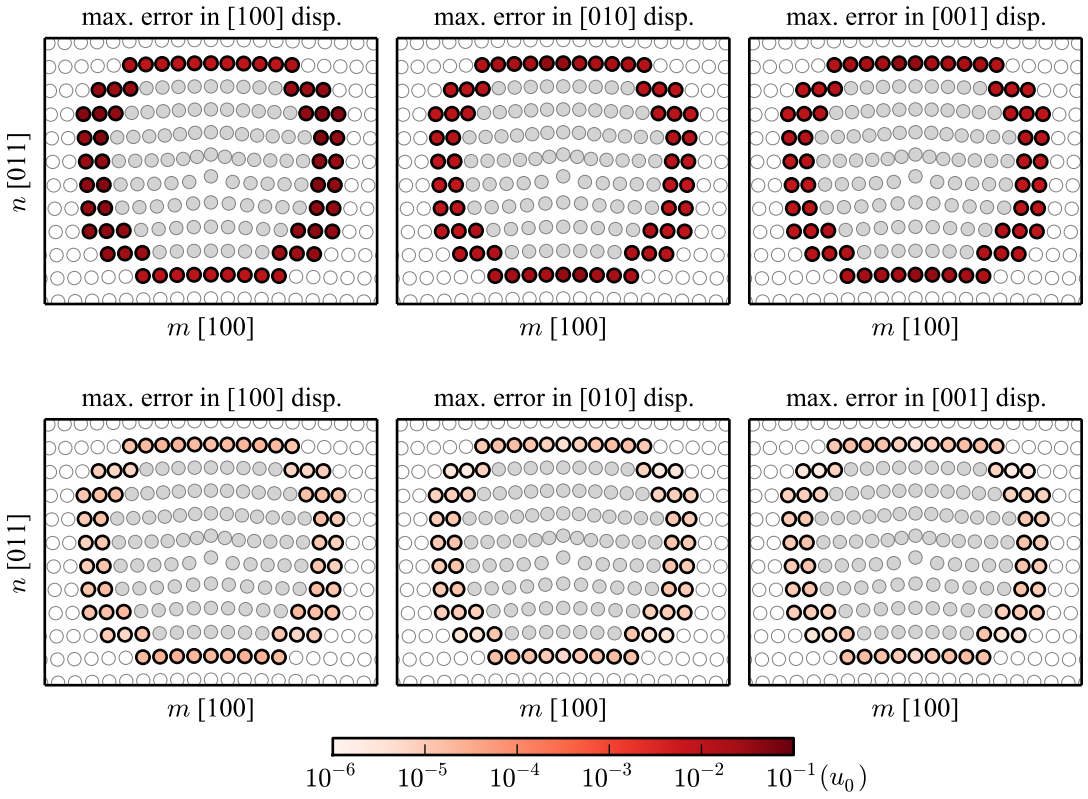

FIG. 6. Maximum error in the displacements generated by the bulk LGF (top) and the edge LGF (bottom) for atoms in a BCC iron $\langle 100 \rangle \{011\}$ edge dislocation geometry. We only apply initial displacements on those atoms which generate no forces in region 3 or beyond (atoms outlined in black). For each of these atoms, the intensity of the shading indicates the maximum error in the displacements computed in response to a set of forces that were originally generated from applying a displacement u_0 in the [100] direction on that atom. The errors in the displacements are proportional to the initial displacement u_0 as we carry out this test in a "harmonic approximate BCC iron" system. Both the bulk and edge LGF were calculated using system size $R = 50a_0$, and the edge LGF was computed using the bulk-like approximation for force-constants. The atoms outlined in grey provide context for the location of the atoms of interest within the system; atoms in region 1 are filled in with grey while the unfilled/white atoms are other atoms in region 2. The errors in the top figure (using the bulk LGF) are $\approx 5.0 \times 10^{-2} u_0$, while the errors in the bottom figure (using the edge LGF) are more than 3 orders of magnitude smaller, $\approx 2.5 \times 10^{-5} u_0$.

from relaxation with fixed boundaries. We use a similar procedure as we used to relax the edge dislocation in the SC system, except this time we perform the conjugate gradient relaxations of region 1 using LAMMPS. We compute the fully relaxed geometry by carrying out a fully atomistic relaxation of the same edge dislocation geometry using fixed boundary conditions, which requires a much larger simulation box containing almost 100,000 atoms. The geometries we obtain from the FBC relaxations using less than 1000 atoms agree well with this fully relaxed geometry, with the difference in atomic positions being on the order of 10^{-3} Å. The accuracy of the geometries relaxed with FBC is limited by forces on the order of 10^{-3} eV/Å that remain in region 3 at the end of the relaxation, as the FBC approach does not relax forces in region 3. This effectively sets a practical limit for the relaxation of forces in regions 1 and 2 to $\approx 10^{-3}$ eV/Å as well.

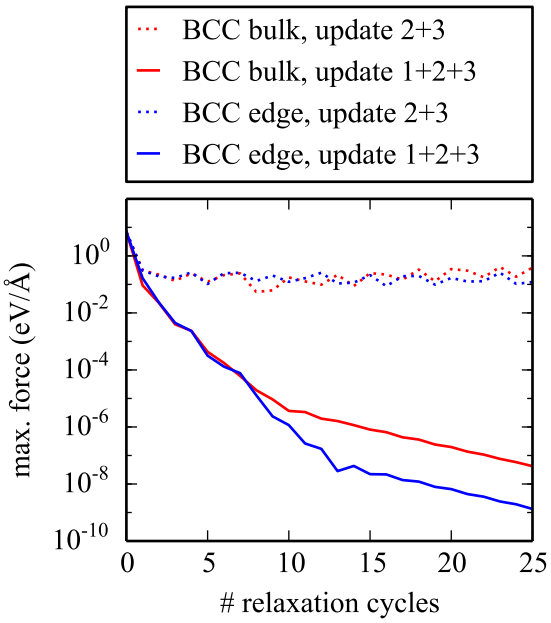

FIG. 7. Comparison of the relaxation of the BCC Fe edge dislocation geometry using different LGF. Both the bulk and edge LGF used during the relaxations were calculated using system size $R = 50a_0$, and the edge LGF was computed using the bulk-like approximation for force-constants. When we include region 1 in the LGF relaxation step (solid lines), the forces in regions 1 and 2 decrease and the geometries converge to the relaxed geometry, with the edge LGF (blue) resulting in faster convergence than the bulk LGF (red). Excluding region 1 in the LGF update step (dotted lines) leads to a failure to converge.

Figure 7 compares the FBC relaxation of the BCC Fe edge dislocation using the bulk and edge LGF, and shows that using the edge LGF to displace atoms in regions 1, 2 and 3 during the LGF update step leads to fastest convergence to the relaxed geometry. When the atoms in regions 1 are fixed during the LGF update step, the relaxations do not converge or do so very slowly. Therefore, even though the LGF may not give accurate displacements for atoms close to the dislocation core, displacing atoms in region 1 according to the LGF in response to forces in region 2 is still more effective than not displacing them at all during this step of the relaxation. When we use either the bulk or the edge LGF to displace atoms in regions 1, 2 and 3 during the LGF update step, the relaxations converge. Both relaxations initially proceed at a similar rate until the forces in regions 1 and 2 are $\approx 10^{-5}$ eV/Å, after which they start to deviate and the relaxation with the edge LGF performs better. For practical purposes the FBC relaxation is typically only carried out until the forces in regions 1 and 2 are $\approx 10^{-3}$ eV/Å, and the bulk and edge LGF both seem to perform similarly up to this point in the relaxation. To better understand the reason for this, we take a more detailed look at the forces in regions 1 and 2 during the first few relaxation cycles.

Figure 8 compares the evolution of forces in regions 1 and 2 during the initial stages of relaxing the BCC Fe edge dislocation geometry, which illustrates how the choice of LGF affects the LGF update steps as well as the overall relaxation behavior. In addition to the bulk LGF and the bulk-like edge LGF, we also compare the behaviors of the edge LGF computed from the strained, strained and rotated, and full dislocation force-constants. To compare the effectiveness of the different LGF at reducing forces during each LGF update, we track the forces after each conjugate gradient (CG) relaxation of the core and after every LGF update. As expected for FBC relaxations, after each CG relaxation, forces in region 1 decrease while forces build up in region 2, and after each LGF update, forces in region 2 decrease but those in region 1 increase slightly. The LGF computed using more accurate force-constants are more effective at relaxing the forces in region 2 during each LGF update, but these effects do not carry over to subsequent steps in the relaxation. After the next CG relaxation, the forces in region 2 increase in all cases to about the same level again, indicating that these forces are mostly due to the rearrangement of atoms in region 1 during the CG relaxation rather than the previous LGF update. We find that all the harmonic approaches are similarly limited during the first few relaxation cycles when forces and displacements are large enough that anharmonic effects are likely to be significant. For this BCC Fe edge

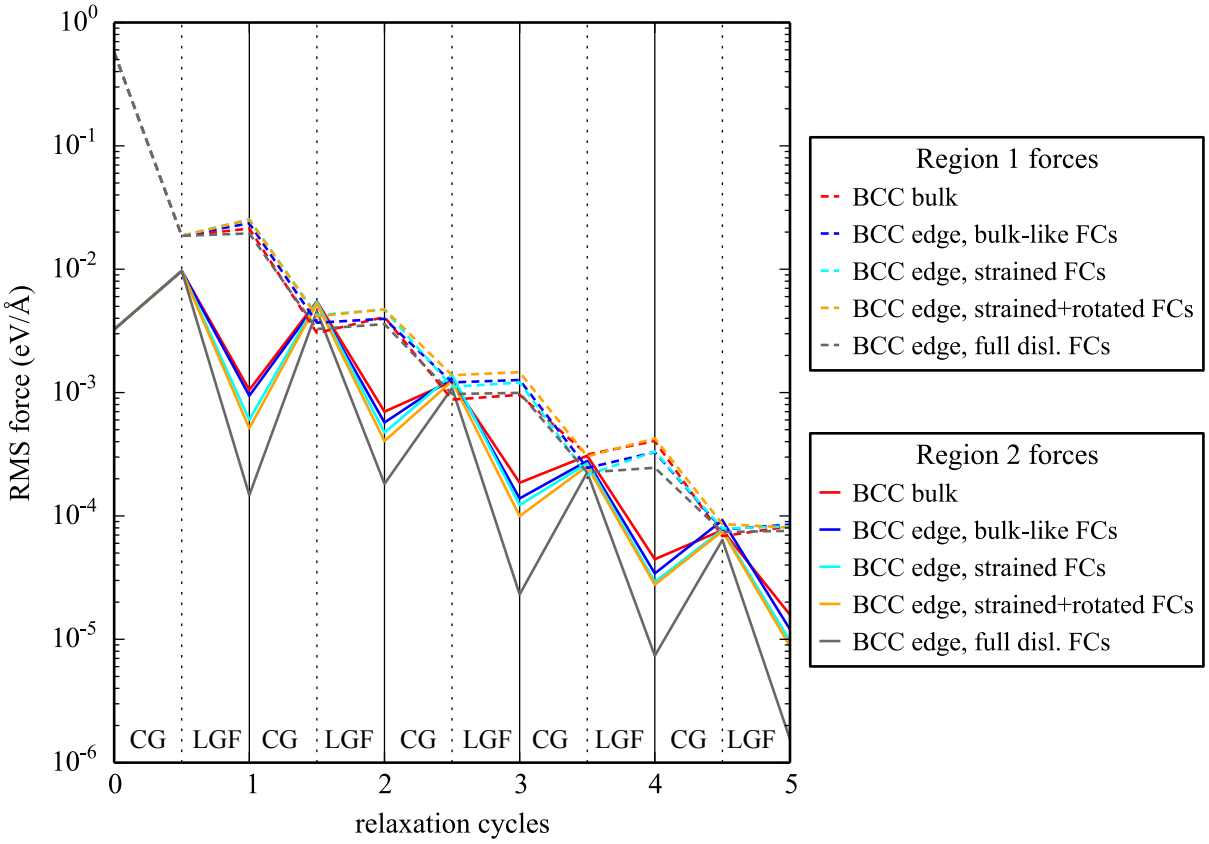

FIG. 8. Comparison of the root-mean-square forces in region 1 and region 2 during the first 5 relaxation cycles, when we relax the BCC Fe edge dislocation geometry using different LGF. In addition to the bulk LGF (BCC bulk; red) and edge LGF computed using the bulk-like force-constants (BCC edge, bulk-like FCs; blue), we also consider the edge LGF where we account for local strain (BCC edge, strained FCs; cyan) and local strain and rotation (BCC edge, strained+rotated FCs; orange), as well as the edge LGF computed using the full dislocation force-constant matrix (BCC edge, full disl. FCs; grey). Each relaxation cycle consists of two steps—relaxing atoms in the region 1 by CG, followed by displacing atoms in regions 1, 2 and 3 according to the LGF. During the CG relaxation, forces in region 1 (dashed lines) decrease while those in region 2 (solid lines) increase. This trend is reversed during the LGF update step. The LGF computed using more accurate force-constants are slightly more effective at relaxing the forces in region 2 after each LGF update step. However, these differences in behavior during each LGF update do not carry over to subsequent steps in the relaxation.

dislocation, the effect of topology only becomes evident later on in the relaxation, while the different approximations for the force-constants have an even smaller effect on the computed LGF and overall relaxation behavior. For more complicated geometries that deviate more greatly from bulk—such as dislocations in multiple atom basis crystals which have larger Burgers vector—the topology effect could become significant earlier on in the relaxation than we observe in this particular system. If that is the case, we expect that using the edge LGF would lead to more noticeable improvement in the relaxation even in the first few relaxation cycles.

Figure 9 shows that the errors in both the computed LGF and the relaxed BCC Fe edge dislocation geometries converge as $1/R^2$. As we did for the SC case, we compute the LGF using different system sizes R and extrapolate the data to estimate the LGF as $R \to \infty$. The figures plot the convergence of the edge LGF computed using the bulk-like approximation for the force-constants; we also find similar behavior for the edge LGF computed using the other methods for approximating the force-constants. The errors in the LGF are small (on the order of $10^{-4}\text{Å}^2/\text{eV}$), controllable, and converge rapidly as $1/R^2$, which again suggests that the approximation we used in the far-field is appropriate. Again, we also compare the edge dislocation geometries obtained after relaxation with FBC using edge LGF computed with different R. We calculate the differences in the relaxed geometries obtained from relaxations using LGFs computed with $R = 15a_0, 20a_0, 30a_0, 40a_0$ compared to that obtained from using the LGF computed with $R = 50a_0$. The differences in the relaxed geometries are small (on the order of 10^{-5} Å) and converge rapidly as $1/R^2$. These results show that the LGF can be computed accurately using small system sizes and with low computational cost.

VI. CONCLUSION

We present a numerical method for computing the LGF specifically for a dislocation geometry, and show that the efficiency of FBC approaches can potentially be improved by using the LGF computed with this method. We have applied our method for computing the dislocation LGF to two systems—a simple cubic model system and BCC iron—each containing an edge dislocation. The errors in the LGF computation converge rapidly with system size in both cases. By directly accounting for the topology of the dislocation, the dislocation LGF is able to capture the response of atoms in the dislocation geometry more

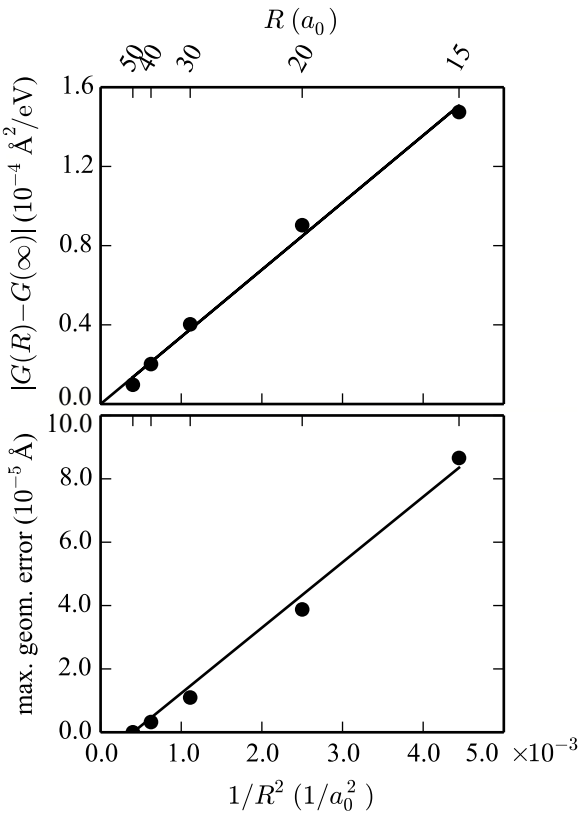

FIG. 9. Convergence behavior of the errors in the computed G (top) and the relaxed edge dislocation geometry (bottom) for the BCC Fe system, with respect to system size R. In each figure, the solid line is the best-fit line through the data points (filled circles). (Top) The vertical axis is the deviation of $G(R = 15a_0, 20a_0, 30a_0, 40a_0, 50a_0)$ from $G(R \to \infty)$. The figure plots the convergence of one specific entry of G; we found that other entries of G show similar convergence behavior as well. (Bottom) The vertical axis is the maximum difference between the geometries obtained from relaxation using $G(R = 15a_0, 20a_0, 30a_0, 40a_0)$ compared to that obtained from using $G(R = 50a_0)$. Both the errors in the computed G and the relaxed edge dislocation geometry are small and demonstrate close to $1/R^2$ convergence behavior.

accurately than the perfect bulk LGF. When used within the flexible boundary condition approach, the dislocation LGF relaxes dislocation core geometries in fewer iterations than when the bulk LGF is used. We expect to see even greater improvement in the efficiency of FBC relaxations if the dislocation LGF is used to relax more complicated geometries, such as dislocations in multiple atom basis crystals which have larger Burgers vector or dislocations in grain boundaries. Reducing the number of iterations needed to relax dislocation core

geometries by using the dislocation LGF would greatly benefit density functional theory based FBC approaches which are computationally expensive.

ACKNOWLEDGEMENTS

This research was supported by NSF/DMR Grant No. 1410596.

---

[1] P. Haasen, *Physical Metallurgy*, 3rd ed., edited by J. Mordike (Cambridge University Press, Cambridge, 1996).

[2] A. Stroh, J. Math. Phys. **41**, 77 (1962).

[3] D. J. Bacon, D. M. Barnett, and R. O. Scattergood, Prog. Mater. Sci. **23**, 51 (1980).

[4] C. Woodward, Mater. Sci. Eng., A **400-401**, 59 (2005).

[5] T. A. Arias and J. D. Joannopoulos, Phys. Rev. Lett. **73**, 680 (1994).

[6] S. L. Frederiksen and K. W. Jacobsen, Philos. Mag. **83**, 365 (1994).

[7] J. R. K. Bigger, D. A. McInnes, A. P. Sutton, M. C. Payne, I. Stich, R. D. King-Smith, D. M. Bird, and L. J. Clarke, Phys. Rev. Lett. **69**, 2224 (1992).

[8] S. Ismail-Beigi and T. A. Arias, Phys. Rev. Lett. **84**, 1499 (2000).

[9] E. B. Tadmor, M. Ortiz, and R. Phillips, Philos. Mag. A **73**, 1529 (1996).

[10] G. Lu, E. B. Tadmor, and E. Kaxiras, Phys. Rev. B **73**, 024108 (2006).

[11] N. Choly, G. Lu, W. E, and E. Kaxiras, Phys. Rev. B **71**, 094101 (2005).

[12] Z. C. Y. Liu, G. Lu and N. Kioussis, Model. Simul. Mater. Sci. Eng **15**, 275 (2007).

[13] J. E. Sinclair, P. C. Gehlen, R. G. Hoagland, and J. P. Hirth, J. Appl. Phys. **49**, 3890 (1978).

[14] P. Giannozzi, S. de Gironcoli, P. Pavone, and S. Baroni, Phys. Rev. B **43**, 7231 (1991).

[15] L. Pastewka, T. A. Sharp, and M. O. Robbins, Phys. Rev. B **86**, 075459 (2012).

[16] D. T. Read and V. K. Tewary, Nanotechnology **18**, 105402 (2007).

[17] C. Woodward and S. I. Rao, Phys. Rev. Lett. **88**, 216402 (2002).

[18] C. Woodward and S. I. Rao, Philos. Mag. A **81**, 1305 (2001).

[19] C. Woodward, D. R. Trinkle, L. G. Hector, and D. L. Olmsted, Phys. Rev. Lett. **100**, 045507 (2008).

[20] J. A. Yasi, L. G. Hector, and D. R. Trinkle, Acta Mater. **59**, 5652 (2011).

[21] V. K. Tewary, Adv. Phys. **22**, 757 (1973).

[22] I. R. MacGillivray and C. A. Sholl, J. Phys. F **13**, 23 (1983).

[23] D. R. Trinkle, Phys. Rev. B **78**, 014110 (2008).

[24] J. A. Yasi and D. R. Trinkle, Phys. Rev. E **85**, 066706 (2012).

[25] M. Ghazisaeidi and D. R. Trinkle, Phys. Rev. B **82**, 064115 (2010).

[26] M. Born and K. Huang, *Dynamical Theory of Crystal Lattices* (Oxford University Press, London, 1954).

[27] A. A. Maradudin, E. W. Montroll, and G. H. Weiss, *Theory of Lattice Dynamics in the Harmonic Approximation*, 2nd ed., Solid State Physics Suppl. 3 (Academic Press, New York, 1971).

[28] V. K. Tewary, Phys. Rev. B **69**, 094109 (2004).

[29] V. Tewary, in *Modeling, Characterization, and Production of Nanomaterials*, Woodhead Publishing Series in Electronic and Optical Materials, edited by V. K. Tewary and Y. Zhang (Woodhead Publishing, 2015) pp. 55 – 85.

[30] A. A. Maradudin, Rep. Prog. Phys. **28**, 331 (1965).

[31] S. Plimpton, J. Comput. Phys. **117**, 1 (1995).

[32] M. I. Mendelev, S. Han, D. J. Srolovitz, G. J. Ackland, D. Y. Sun, and M. Asta, Phil. Mag. A **83**, 3977 (2003).

[33] D. Alfe, Comput. Phys. Commun. **180**, 2622 (2009).